# Hole-initiated melting process of thin films

Chenyu Jin[1, a)] and Hans Riegler[1, b)]
*Max Planck Institute of Colloids and Interfaces, Science Park Golm, 14476 Potsdam, Germany*

(Dated: 26 April 2022)

It is generally believed that melting of a thin film starts from a small defect, e.g., a hole on the film that acts as the nucleation site. We show in this study that when the contribution of the capillary surface (liquid/air interface) is taken into consideration, the melting process is non-trivial: 1) There may be multiple melting pathways for one system, and hence different "de facto" melting points. 2) Melting of a thin film may start from the long, straight edge rather than the small holes if the edge facet wets better than the substrate. This is verified by experimental data from melting alkane layers between silica and air. Our findings provides a general approach for solving the non-trivial melting scenarios in systems with capillary surfaces.

PACS numbers: 36.40.Ei, 64.70.dj, 68.08.Bc

## I. INTRODUCTION

Thermostability of thin films is of great interest in theory and in practice[1]. For example, it is very important to know when and how an anti-corrosion coating, a filter membrane, or a semi-conductor layer, would collapse under high temperature. Generally, we are to look into the melting process of the thin film: in such a confined system, the "de facto" melting point is different from the melting point of the bulk material, due to the ineligible contribution from the interfacial free energies.

The classical description of melting under confinement is based on a two-phase system: a small solid particle covered by its melt, with one solid-liquid interface. The area of this interface varies during melting, hence the interfacial energy varies and contributes to the total free energy change. Melting point shift calculated with this model is the Gibbs-Thomson equation widely used by experimentalists and engineers[2–5]. For the thin films, a variation of this model is used, but same as the original model, only the solid-liquid interface is considered.

However, in most real cases, there will be at least one capillary surface, i.e., the liquid-air interface. The prerequisite of the Gibbs-Thomson equation is that the liquid melt completely covers the solid particle floating in the air, so that the capillary surface is a spherical shell that doesn't change in shape or area. In practice, this means all the facets of the floating particle must be "premelting"[6,7], i.e., a thin layer of liquid melt covers the solid facets BEFORE the temperature reaches the bulk melting point. A bad news is that "premelting" is only confirmed on certain facets of ice and lead (Pb). Experimental study with lead particles shows that the Gibbs-Thomson equation breaks down once a non-premelting facet is involved, i.e., the liquid melt wets the facet with a non-zero contact angle[8]. This will also happen when the particle is not floating but in contact with a substrate. Liquid could be pinned at the grain boundaries, or wet the substrate with a non-zero contact angle. The shape of the capillary surface will become non-trivial, so does the interfacial energy. For long it has been known that the effects of the capillary surface on melting is complex[9–13]. But still, this problem is rarely systematically analysed.

Previously, we have observed an unexpected melting scenario of molecularly thin terrace of long-chain alkanes: liquid drops appear at the edge and "eat" into the terrace[14]. We have revealed that the emergence of these drops is due to the Plateau-Rayleigh instability of the capillary surface[15]. Later we have analysed the melting behaviour of cylindrical aggregates[16] in gaseous environment based on the same experimental system, and have calculated the deviation of the "de facto" melting point from Gibbs-Thomson equation due to the capillary surface.

In this work, we study the melting behaviour of a thin, planar solid film from a defect in the shape of a cylindrical hole. We show that the melting scenario may include a morphology transition of the capillary surface, and the morphology of the capillary surface will decide the melting path as well as the "de facto" melting point of the system. Although the simulation is based on our experimental system of long-chain alkane film between air and silica substrate, the model is easily generalised to other systems.

## II. THEORY AND METHODS

### A. Thermodynamics

We analyze the melting process in a continuum approach.[17]. Contributions from the line tension[18,19], the disjoining pressure[20], and the gravity are neglected. When alkane solid melts, the volume increase typically by $\approx 10\%$[21]. This change in volume can be neglected without changing our conclusion. We hence use the volume of the liquid melt $V_\mathrm{l}$ to represent the amount of the

[a)] Present address: Uni Bayreuth, Univertitätstr. 30, 95447, Bayreuth; Electronic mail: dr.chenyu.jin@gmail.com
[b)] Electronic mail: Hans.Riegler@mpikg.mpg.de

material that undergoes melting.

In this study, we focus on the slow, equilibrated process: the capillary surface is always fully relaxed to the minimum of the interfacial energy (area), and the energy fluctuation is generally not taken into consideration hence metastable states are allowed. The system status is determined by the total free energy, which is the sum of the contributions from the bulk energy $G_{\mathrm{B}}$ and the interfacial energies $G_{\mathrm{I}}$. If we heat up the system to an arbitrary temperature $T$, the system will adjust to the new thermodynamic equilibrium. For example, some solid may melt ($V_{\mathrm{l}}$ increases) until the total free energy is minimized. At equilibrium we always have

$$\frac{dG_{\mathrm{total}}}{dV_{\mathrm{l}}} = \Delta\mu + \frac{dG_{\mathrm{I}}}{dV_{\mathrm{l}}} = 0 \tag{1}$$

where $\Delta\mu$ is the bulk chemical potential difference per volume between liquid and solid under a constant pressure (in this case, 1 bar).

Gibbs free energy is the indicator for the direction of a process: if $G_{\mathrm{total}}$ decreases ($dG_{\mathrm{total}}/dV_{\mathrm{l}} < 0$), then the process proceed forward; if increases, then backward. In Eq. (1), $\Delta\mu$ only depends on the temperature $T$. But $dG_{\mathrm{I}}/dV_{\mathrm{l}}$ does not change with $T$, rather it is a function of $V_{\mathrm{l}}$. If we know these two functions, we can predict the melting scenario of the system from any arbitrary $T$ and $V_{\mathrm{l}}$, given that $V_{\mathrm{l}}$ naturally increases when melting proceeds. For example, if the system starts with a $(T, V_{\mathrm{l}})$ where $dG_{\mathrm{total}}/dV_{\mathrm{l}} < 0$, the system will start to melt and $V_{\mathrm{l}}$ increases, then:

- if $dG_{\mathrm{I}}/dV_{\mathrm{l}}$ decreases, $dG_{\mathrm{total}}/dV_{\mathrm{l}}$ is always negative, melting continues;
- if $dG_{\mathrm{I}}/dV_{\mathrm{l}}$ increase, $dG_{\mathrm{total}}/dV_{\mathrm{l}}$ will approach 0. Melting will stop at another $V_{\mathrm{l}}$ that makes $dG_{\mathrm{total}}/dV_{\mathrm{l}} = 0$. Note that in this case, the solid will coexist with some amount of liquid melt.

Following we will have a look at the exact function for $\Delta\mu$ and $dG_{\mathrm{I}}/dV_{\mathrm{l}}$.

As the relevant temperature range is often small, a constant melting entropy $\Delta S_{\mathrm{fus}}$ can be assumed. $\Delta\mu$ at an arbitrary temperature $T$ is calculated as[22,23]

$$\Delta\mu \simeq -\Delta S_{\mathrm{fus}} \cdot (T - T_0) \tag{2}$$

$T_0$ is the bulk melting point. $\Delta\mu$ decreases linearly with the temperature $T$: the higher $T$ is, the more negative $dG_{\mathrm{B}}$ is.

In a simple system described by the Gibbs-Thomson model, i.e., a small spherical solid particle (radius $r_0$) covered with liquid melt (solid-liquid interfacial tension $\gamma_{\mathrm{sl}}$). $dG_{\mathrm{I}}/dV_{\mathrm{l}} = -2\gamma_{\mathrm{sl}}/(r_0^3 - 3V_{\mathrm{l}}/(4\pi))^{1/3}$ is a strictly decreasing function over the change of $V_{\mathrm{l}}$. Hence there will not be co-existence of the solid and liquid: once the temperature is above a certain $T_{\mathrm{m}}$, so that $dG_{\mathrm{total}}/dV_{\mathrm{l}} < 0$ at $V_{\mathrm{l}} = 0$, melting will complete instantly.

However, because of the non-trivial shape of the capillary surface, the function for $dG_{\mathrm{I}}/dV_{\mathrm{l}}$ of $V_{\mathrm{l}}$ is also non-trivial.[24] For example, in Fig. 3(b), $dG_{\mathrm{I}}/dV_{\mathrm{l}}$ first rises with $V_{\mathrm{l}}$. As a result there will be a small temperature range inside which the liquid melt co-exists with the solid. This co-existence can be stable or metastable, and was reported in our previous studies[15,16].

With Eq. (1) and Eq. (2), we can deduce that the "equilibrium" temperature $T_{\mathrm{eq}}$ is related to the "equilibrium" volume $V_{\mathrm{l}}^{\mathrm{eq}}$ as:

$$T_{\mathrm{eq}} - T_0 = \frac{1}{\Delta S_{\mathrm{fus}}} \cdot \left(\frac{dG_{\mathrm{I}}}{dV_{\mathrm{l}}}\bigg|_{V_{\mathrm{l}}=V_{\mathrm{l}}^{\mathrm{eq}}}\right) \tag{3}$$

Naturally, the upper limit of $T_{\mathrm{eq}}$ corresponds to the maximum of $dG_{\mathrm{I}}/dV_{\mathrm{l}}$. This is the temperature under which the system will melt completely without any energy barrier. We call it the "de facto" melting temperature $T_{\mathrm{m}}$ of the system.[25] As shown in Fig. 3(b), in our system $dG_{\mathrm{I}}/dV_{\mathrm{l}}$ increases and then decreases with $V_{\mathrm{l}}$, hence the liquid volume $V_{\mathrm{eq}}$ at $T_{\mathrm{m}}$ is also the maximum. It characterize the maximum coexistence liquid volume beyond which the system melt completely. We write it as $V_{\mathrm{m}}$.

$$\Delta T_{\mathrm{m}} = T_{\mathrm{m}} - T_0 = \frac{1}{\Delta S_{\mathrm{fus}}} \cdot \left(\frac{dG_{\mathrm{I}}}{dV_{\mathrm{l}}}\right)_{\max} \tag{4}$$

Therefore, in order to solve the melting scenario of a system, one approach is: First look into various intermediate states during melting, relax the capillary surfaces and calculate the free energies. Then get the function for $dG_{\mathrm{I}}/dV_{\mathrm{l}}$ of $V_{\mathrm{l}}$ by connecting these states into melting pathways. The whole melting scenario could then be constructed as shown in the following sections.

### B. Simulation details

We focus on the melting of a film between two different media: a substrate and air. Melting of a film between two identical media or substrates is either straight-forward to analyze, or closed related to what we analyze here. A cylinder hole (radius $r_0$) penetrating the film until the substrate is where the melting would start. For calculation we assume the followings:

- The hole maintains a smooth, right cylinder geometry. The substrate is planar and the film is of uniform thickness, hence the hole also maintains a constant height $h$ during melting;
- The total volume of solid and liquid phase together remains constant as the density difference between solid and liquid is neglected;
- The liquid wets completely the side walls of the cylindrical hole, but only partially the film surfaces and the substrates, with a non-zero contact angle;

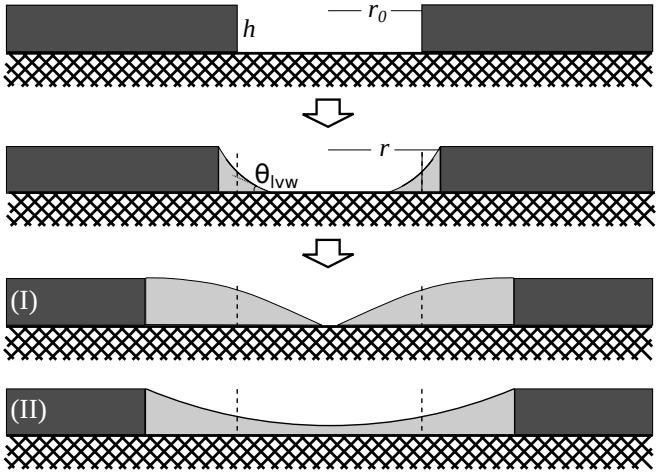


FIG. 1. Melting scenario from a hole of finite size in an infinite film of uniform thickness. The solid walls are assumed cylindrical and perpendicular during melting. The melt completely wets the side walls. The substrate is wetted only partially with contact angle $\theta_{ls}$. Different amounts of liquid melt (corresponding to different temperatures) will lead to different liquid morphologies such as and open channel (I) or a closed concave film (II).

- The liquid is "pinned" at the solid/air/liquid contact line of the hole edge, meaning that there is no fixed contact angle at this line;
- Young's equation holds for contact angles at the liquid/substrate/air contact lines.

The non-trivial shape of the capillary surface during the melting is solved by relaxing the surface in Surface Evolver[26] with each arbitrary $V_l$ and corresponding boundary conditions. For the simulations we use real data of long-chain alkane systems[27–29]: $\gamma_{lv} = 25 \times 10^{-3}$N/m, $\gamma_{lw}$(hole side wall) $= 10 \times 10^{-3}$N/m, $\gamma_{ls}$(film surface and substrate) $= 4 \times 10^{-3}$N/m, and $\Delta S_{fus} = 5 \times 10^5$ J/Km$^{-3}$. The contact angle is $\theta_{ls} = 15°$ on both the film surface and the substrate. The model can be easily tuned to simulate different systems. For example, if use $\theta_{ls} = 90°$, the model represents not only a film coated on a substrate, but also half of a self-supporting film in the air.

Fig. 1 illustrates the different liquid morphologies that may emerge during melting at a round hole in a planar film. The holes have a radius $r_0$ in the all-solid case (at $T \ll T_0$) and a depth $h$ (same with the film thickness). When some solid melt into the liquid state, the radius of the hole is $r$, the liquid volume $V_l = \pi h(r^2 - r_0^2)$. Upon increasing temperature liquid melt will first appear as a uniform channel at edge of the hole. To be exact, the capillary surface will be a rotational-symmetric constant-mean-curvature surface (Delaunay surface, or rouloid)[30,31]. As the liquid volume increases, two distinctively different morphologies are possible: a ring-like channel of the liquid with a opening in the center exposing part of the bare substrate ("open" shape, (I)), and a spherical concave covering the entire substrate ("closed" shape (II)). In (I) the liquid meet the substrate at contact angle $\theta_{ls}$.

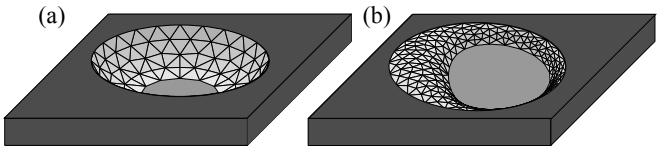


FIG. 2. Two types of "open"morphologies: (a) rouloid and (b) bulged channel .

There is a geometric limit for the "closed" shape: It will only appear when a certain volume of the solid has melted. This lower limit can be calculated analytically as the top surface of the liquid is a concave spherical cap whose edge pinned at the upper rim. Calculation results in a minimum radius $r = r_{min}$ of a hole that can be filled with a liquid concave from melting the solid film:

$$\frac{r_{min}}{h} = \sqrt{2(\frac{r_0}{h})^2 - \frac{1}{3}} \tag{5}$$

Note that this limit is different for very small/deep holes with $r_0/h < 1$, where the liquid front on the substrate closes before the liquid front on the wall can be pinned at the hole edge.

In some cases, typically when a large amount of liquid accumulate at a long edge, there are two possible "open" morphologies (Fig. 2), which are (a) uniform channels and (b) bulged morphologies in isobaric (isocurvature) coexistence with channel sections[15,16]. In this work, mostly the bulged morphologies are only possible at such large $V_l$ (i.e. comparatively high temperatures) that typically the systems already gets absolutely unstable, as will be shown in later analysis. Hence only the morphology transition between the "open" channel and the "closed" concave affects the melting.

In the following, we shall use normalized variables: $\overline{G} = G/(\gamma_{lv} r_0 h)$, $\overline{V} = V/(\pi r_0^2 h)$, $\overline{r} = r/h$, $\overline{\Delta T} = \Delta T \cdot h$, and the in-plane curvature $\overline{\kappa} = \kappa \cdot h$.

### C. Experimental methods

We use silicon wafer covered with a 300 nm thick oxide layer as substrate. The oxide layer has a close refractive index to the long-chain alkane. Such a thickness is chosen because it provides interference enhancement of contrast from thin alkane layers on the substrate[32]. We coat the piranha-cleaned wafer with long-chain alkane (triacontane $C_{30}H_{62}$ or hexatriacontane $C_{36}H_{74}$) solution in toluene. After a heat-cool cycle, a "surface frozen" alkane monolayer[33] will be formed on the wafer. The sample is then annealed at one of two degree below $T_0$ for a few minutes. Films and islands of various size and height will form. The suitable ones are chosen for the melting experiments. The height of the alkane films are measured with atomic force microscope (AFM).

The substrate in such a system is actually the surface frozen alkane monolayer, covering the silica surface. This layer, same with the top of alkane film, can only be partially wetted by liquid alkane melt with a contact angle around $15^o$. This contact angle is directly calculated from microscope observation or alkane droplets: The light (peak wavelength 550 nm) reflected from liquid-air interface and the silica-silicon interface in the wafer will interfere. From the Newton's rings we get the droplet surface profile, and from fitting a circle to the profile we can get the contact angle.

## III. DISCUSSIONS

### A. Transitions between different morphologies during melting

Melting process is characterized by the increase in the volume of liquid melt $\overline{V_l}$. Fig. 3 shows the change of the interfacial free energy $\overline{G_I}$ and $\overline{dG_I/dV_l}$ as the liquid volume increases. The data represent the melting process of a film from a hole of $\overline{r_0} = 5$ on a substrate with $\theta_{ls} = 15^o$. This corresponds to the real cases of holes of about 500 nm in radius in an alkane film of with $h = 100$ nm.

At the bulk melting temperature $T_0$, $G_{total} = G_I$. $\overline{G_I}$ first decrease with $\overline{V_l}$, this means liquid melt already appears and co-exists with the solid at $T_0$. Following our previous analysis, the same conclusion can be read from Fig. 3(b): Starting from $(T_0, 0)$, $\Delta\mu = 0$ so that $d\overline{G_{total}}/d\overline{V_l} < 0$, the system will melt. Then, because $\overline{dG_I/dV_l}$ increases with $\overline{V_l}$, melting will stop at an equilibrium volume $\overline{V_l^{eq}}$, in exact, the volume when the $\overline{dG_I/dV_l} = 0$

Geometrically, the minimum volume for the "closed" shape $\overline{V_{min}} \approx 1$ according to Eq. (5), indicated by **A** on Fig. 3. **B** and **E** indicate the two iso-energy points: After **B** the "closed" shape becomes more favorable in energy; above **E**, the "open" shape becomes more favorable in energy again. Between **C** and **D**, the "open" shape is forbidden.

Combining the energy and geometry analysis, we have such a general melting scenario: If the melting proceeds always with the lowest free energy, it will start from a uniform channel, then the liquid will close into a concave at **B**. The closed liquid concave will rapture into "open" channel at **E**. However, there is an energy barrier between the two morphologies, hence the first morphology transition may happen anywhere between **A** and C. In addition, once $\overline{dG_I/dV_l}$ reaches the maximum and starts to decrease, the system will melt completely, hence the morphology change around **D** and **E** will be barely noticeable.

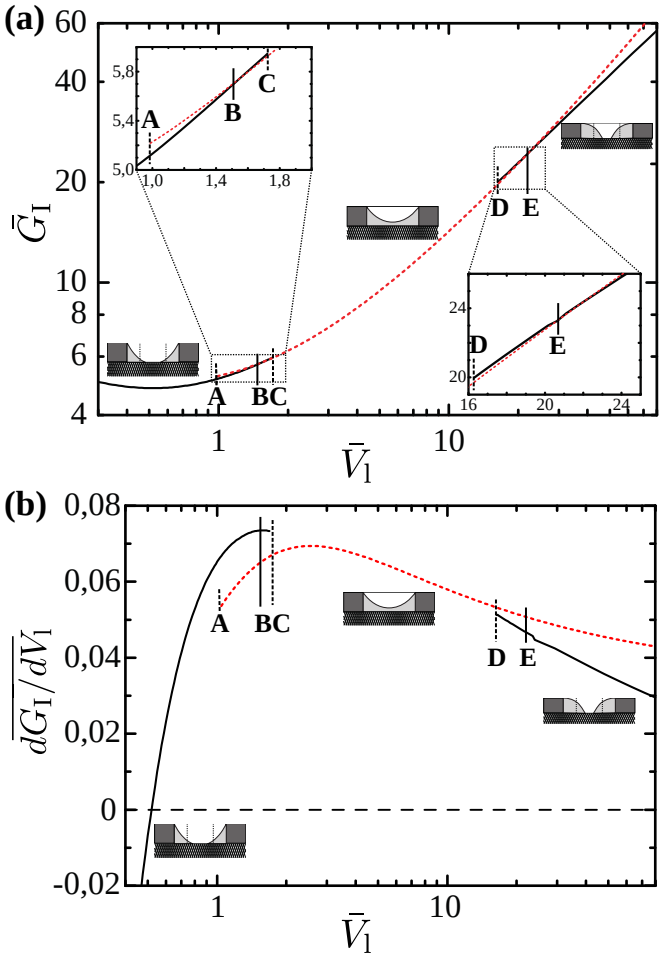


FIG. 3. Melting process of a film from a hole of $\overline{r_0} = 5$ on a substrate with $\theta_{ls} = 15^o$. (a) Interfacial energy $\overline{G_I}$ as a function of liquid volume $\overline{V_l}$. The solid black lines indicate "open" shape, while the dashed lines the closed concave. For small volumes (left of **A**) only uniform channels are possible, for intermediate volumes (between **C** and **D**) the hole can only be filled with a closed concave film. Between **A** and **C**, also above **D**, both morphologies are possible but with a difference in energy. **B** and **E** are the two iso-energy points. (b) The corresponding $\overline{dG_I/dV_l}$ as a function of $\overline{V_l}$.

### B. Melting scenarios and blurred melting points

Following we show how to read the melting scenarios from the $\overline{dG_I/dV_l}$ to $\overline{V_l}$ plots, and analyze the $T_{eq}$, $T_m$ and $V_m$. In Fig. 4 we plot $\overline{dG_I/dV_l}$ to $\overline{V_l}$, for different $\overline{r_0}$ and $\theta = 15^o$. Different $\overline{r_0}$ means the film melt from a hole of different size. **A** to **E** have the same meanings as in Fig. 3. Following Eq. (3) and Eq. (4), in the co-existing temperature range, under equilibrium, $\overline{dG_I/dV_l}$ is proportional to $T_{eq} - T_0$. $\overline{dG_I/dV_l} = 0$ corresponds to the bulk melting temperature $T_0$, and maximize at $(T_m, V_m)$. We could then see the curves, especially the rising part, as system status represented by temperature $T_{eq}$ and liquid volume $V_l$, given that the system is under

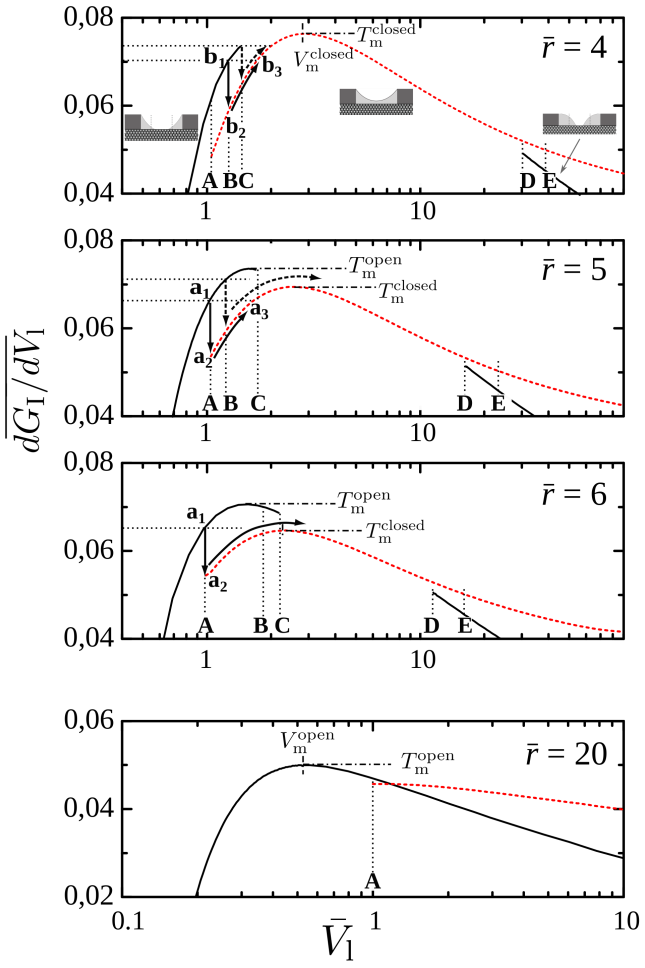


FIG. 4. Melting scenarios of film from holes with different $\overline{r_0}$ and $\theta_{ls} = 15^o$. $\overline{dG_I/dV_l}$ is plotted as a function of the liquid volume scaled to the hole volume, $\overline{V_l}$. Just as in Fig. 3, the solid black lines indicate "open" uniform channels, the dashed red lines closed concaves. Point **A** to **E** have also the same meaning: when the liquid volume is below **A** only uniform channels are possible. Between **C** and **D** the hole can only be filled with a closed concave film. Between **A** and **C**, also above **D**, both morphologies are possible but with a difference in energy. **B** and **E** are the two iso-energy points. $T_m^{open}$ and $T_m^{closed}$ indicate the de facto melting temperatures of the corresponding morphology.

equilibrium. Following the curves we see directly how melting will proceed as the temperature rises slowly.

When $\overline{r_0} = 4$, melting start from liquid forming a uniform channel at the hole edge. Beyond **A** the close concave becomes possible, but its energy is still higher than the uniform channel shape until **B**. Upon the temperature rises, the liquid volume increase as well. The transition from the "open" uniform channel to the closed concave shape may happen somewhere between **A** and **C** by overcoming an energy barrier, or at **C** when the "open" channel shape becomes absolutely impossible and the liquid front coalesce.

Assuming the transition happens at **B**, the iso-energy point. From **b1** to **b2** it will first be an isochoric transition. However, $dG_I/dV_l$ and thus the $T_{eq}$ on the "closed" curve at **b2** is lower than that on the "open" curve at **b1**. If the temperature doesn't change, liquid volume $V_l$ will rapidly increase from **b2** to **b3**. The system is still metastable because the temperature at **b3** is lower than maximum on this curve, $T_m^{closed}$. Even if the transition does not happen until **C**, the system is stable after transition. Hence $T_m^{closed}$ is the only "de facto" melting point in this system.

In practice, this melting scenario means we could seal some small holes in the solid film: We rise the temperature slowly until there is enough liquid inside the hole to form a closed concave, while carefully keep the temperature below $T_m^{closed}$. Then we freeze quickly the system and solidify the closed concave of liquid melt into a glass state, the small hole will be sealed.

When $\overline{r_0} = 5$, the scenario becomes different around the first morphology transition: If the transition occurs already at **A**, it will start from **a1**, goes via **a2** to **a3**. Then the system may remain metastable at **a3** because this $T_{eq}$ is below the maximum on the "closed" curve, $T_m^{closed}$. However, if the transition happens later, e.g., at **B** the iso-energy point, same process will lead to a complete melting as the corresponding temperature is already higher than $T_m^{closed}$. If the morphology transition does not happen, the film will melt when the temperature reaches $T_m^{open}$, the maximum on the "open" curve. This means, the "de facto" melting point $T_m$ of such a system is a temperature range rather than a single temperature point. It can be any temperature between $T_m^{closed}$ and $T_m^{open}$, depending on when the system jumps to the other morphology.

When $\overline{r_0} = 6$, once the morphology transition happens, even at the minimum volume (**A**), temperature is already higher than $T_m^{closed}$, and the whole system will melt immediately. But if the morphology transition does not happen, the film will then melt at $T_m^{open}$. The "de facto" melting point $T_m$ of this system is also a temperature range, but between $T_{eq}^{\mathbf{A}}$ and $T_m^{open}$

In the last case with $\overline{r_0} = 20$, the liquid in the system will stay in uniform channel shape up to $V_m^{open}$, where complete melting starts. A closed liquid concave is only possible after that, hence absolutely unstable in the sense of melting.

### C. Phase diagram of the various morphologies

Combining the analysis of the geometry, the energy, and the stability, we plot in the Fig. 5 a phase diagram of various morphologies. The phase diagram exhibits the melting scenarios of films with holes of different sizes.

Frame (a) depicts the regions where the two different morphologies are (not) allowed due to mechanical and ge-

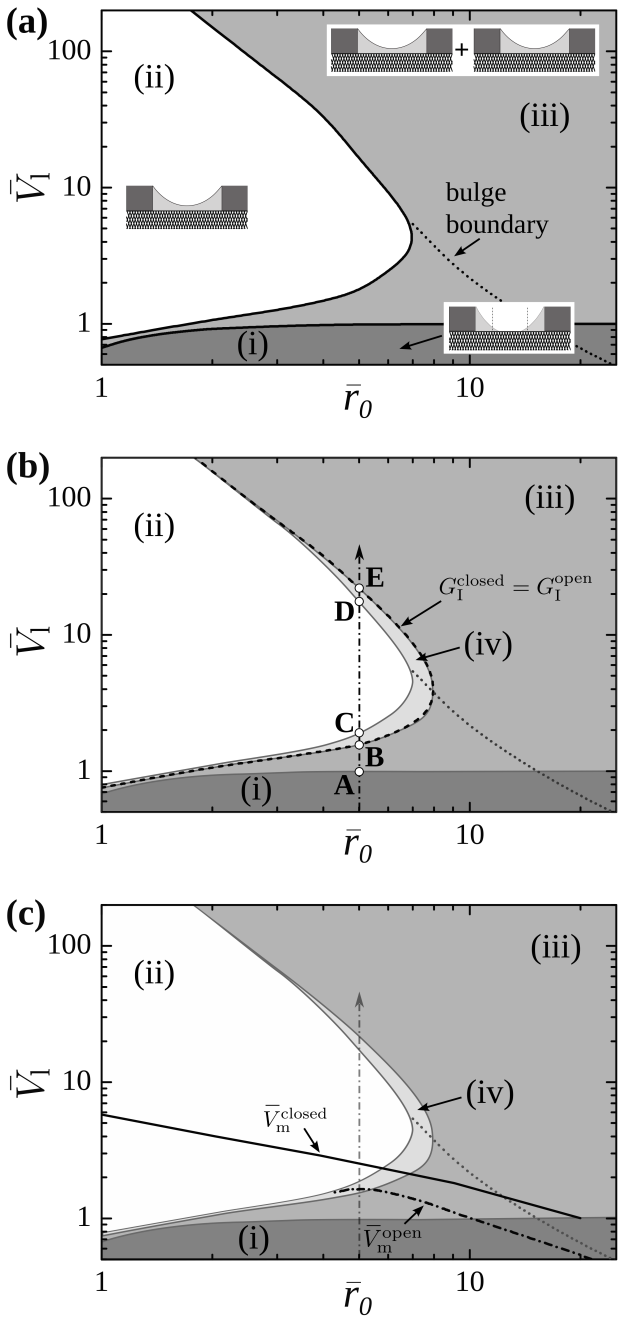


FIG. 5. Phase diagram for the two different morphologies ("open" channel, "closed" concave) in a plot of the liquid volume (scaled to the original hole volume) as function of the original hole radius (scaled to the film thickness). Frame (a) shows regions where only "open" channels (i), only closed concaves (ii), or both morphologies (iii) can exist due to the geometrical boundary conditions ($\theta_{\rm ls} = 15^\circ$, uniform pressure within the liquid). The bulge boundary is also indicated. At volumes above this boundary, open channel shape is still possible, but higher in energy than the bulged channel. Frame (b) includes the curve where the "open" and "closed" morphologies have the same interfacial energy. A volume-increasing path is also indicated, with the **A** to **E** points corresponds to those in Fig. 3. Frame (c) shows the critical volumes of both morphologies, i.e., the absolute volume limits of thermal stability.

ometrical constraints (contact angle, volume, uniform internal pressure). The whole phase diagram is divided into three regions where: (i) only open morphologies are possible, (ii) only closed concaves are possible and (iii) both morphologies are possible. The line separating the region (i) and region (iii) is derived analytically from Eq. (5) All the other data result from numerical simulations with Surface Evolver. The "bulge boundary" divides region (i) and (iii) further into the areas where: a) only uniform channels are possible (volumes below the boundary) and b) both uniform channels and bulged morphologies are possible.

In frame (b) we add the iso-energy boundary, the boundary where open morphologies and closed films have the same interfacial energy ($G_{\rm I}^{\rm closed} = G_{\rm I}^{\rm open}$). The iso-energy boundary separate a small region (iv) from region(iii). The interfacial energy of the closed concave shape is lower than the "open" shape inside region (iv), but higher in the rest part of region (iii). The vertical line at $r_0/h = 5$ shows the same scenario as presented in Fig. 3. The points **B** and **E** lie on the iso-energy boundary, while points **A**, **C**, and **E** lie on the boundaries of regions for certain morphologies.

Finally, in frame (c) we add the absolute thermodynamic stability limits of two morphologies, i.e. the "critical" volumes $V_{\rm m}$. In Fig. 4, these volumes are shown as $V_{\rm m}^{\rm open}$ and $V_{\rm m}^{\rm closed}$, the liquid volume at the "de facto" melting points $T_{\rm m}^{\rm open}$ and $T_{\rm m}^{\rm closed}$.

It should be emphasized that Fig. 5 presents the phase diagram with respect to the (scaled) liquid volume and not with respect to the temperature. The volume increase of the liquid melt after a morphology transition does not show here.

### D. Experimental results of different hole melting scenarios

Combined with our previous calculation on melting of cylindrical island[16] and straight-edge terrace[15], we have now the full picture of melting point shifts of different geometries. In Fig. 6 we plot the scaled melting point shifts $\Delta T \cdot h$ in our model system as the function of the scaled in-plane curvature of the all-solid hole $\overline{\kappa_0} = h/r_0$. We use in-plane curvature instead of radius to distinguish hole and island: hole has negative in-plane curvature $\overline{\kappa_0} = -h/r_0$. The region with two separate lines shows the geometry that can have multiply "de facto" melting points depending on the melting paths. The prediction is that our thin film will start to melt from the long, straight edge rather than the tiny defects (holes) inside the film. This is contradict to the instinct, but is verified by our experiment. Fig. 6 shows the melting process of a alkane film ($C_{36}H_{74}$) in which different geometry can be found: The curved edge behave locally like islands with different radius. Inside the film there are two holes of different size. Top right panel shows that under the same temperature, most liquid appear at the edge (1), around the big hole a significant amount of solid melt as well,

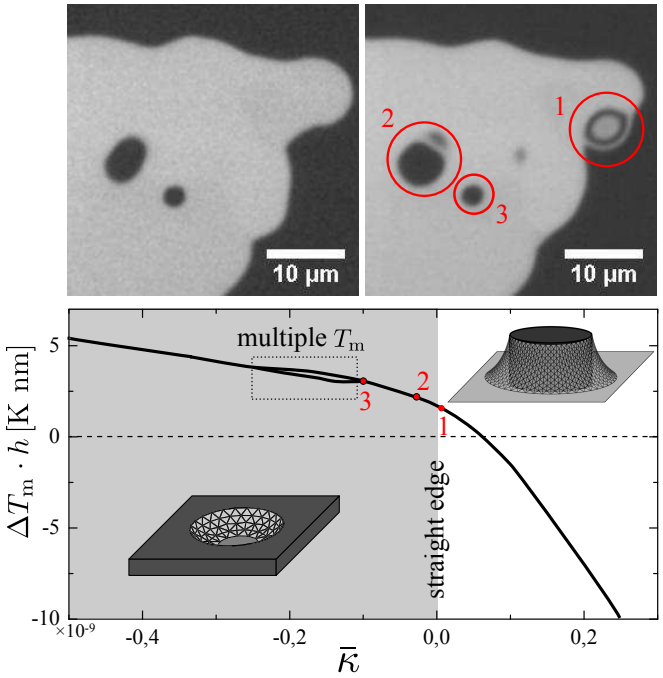


FIG. 6. Top: Melting behavior of solid alkane film ($h \approx 0.1\,\mu$m) with three different local structures: (1) an almost straight edge ($\overline{r_0} \to \infty$); (2) a hole with $\overline{r_0} \approx 30$; (3) a hole with $\overline{r_0} \approx 10$. In the same experiment they melt sequentially. Bottom: Simulated result for alkane film / island melting behavior. Bulging is not included here. Melting point shifts multiplied by film thickness are plotted as the function of the scaled initial in-plane curvature $\overline{\kappa_0}$. Therefore the grey region shows film melting from hole, and the white region shows melting of island. The boundary between the two region indicates melting of a straight terrace edge. Melting point shifts for the three local structures shown in top frame are marked respectively. Dotted rectangular indicates the geometries whose "de facto" melting points are not single temperature, but within an interval as discussed before.

while around the smallest hole (3) barely any change can be observed. Such a melting sequence is consistent with the estimated "de facto" melting points at these three geometries: (1) with the lowest "de facto" melting point melts the first, (3) with the highest "de facto" melting point melts the last.

## IV. CONCLUSIONS

In this work, we have presented an approach to solve the non-trivial melting scenarios in systems with capillary surfaces: first calculate the shape and energy of various intermediate states during melting, connecting them into possible melting pathways, then plot the function for $dG_I/dV_I$ on $V_I$ along each pathway. Under equilibrium, $dG_I/dV_I$ is approximately linear to $T$, hence the plots show the details how the system will melt when temperature rises gradually. This approach is especially useful in unveiling the non-trivial effect of capillary surfaces on the melting of systems.

We analyzed and discussed the melting scenarios of thin films from round holes of different size. The model is built based on the real system of alkane layers between silica and air. Liquid melt wets the substrate and the wall of the hole differently, resulting a capillary surface of various shape: rouloid, bulged channel, and spherical concave. The possible shapes of the capillary surface and its energy are calculated by Surface Evolver, then the possible melting scenarios are constructed. We have found that depending on the system history (melting path), the system may have multiple "de facto" melting temperatures.

Quite contradict to the instinct, our analysis has predicted that in this system (thin films of long chain alkanes between silica and air), a film will melt from a straight edge rather than the small defects (holes). This prediction is supported by experiment results.

## V. ACKNOWLEDGEMENT

Discussion with H. Möhwald, H. Kusumaatmaja are gratefully acknowledged. C.Jin was support from IMPRS on Biomimetic Systems.

[1] P. Huber, Journal of Physics: Condensed Matter **27**, 103102 (2015).
[2] P. Pawlow, Z. Phys. Chem **65**, 1 (1909).
[3] G. Tammann, Z. Anorg. Allg. Chem. **110**, 166 (1920).
[4] F. Meissner, Z. Anorg. Allg. Chem. **110**, 169 (1920).
[5] E. Rie, Z. Phys. Chem. **104**, 354 (1923).
[6] J. W. Frenken and J. Van der Veen, Phys. Rev. Lett. **54**, 134 (1985).
[7] J. Dash, Contemp. Phys. **30**, 89 (1989).
[8] J. Métois and J. Heyraud, J. Phys. France **50**, 3175 (1989).
[9] N. Maeda and H. K. Christenson, Colloids Surf A Physicochem Eng Asp. **159**, 135 (1999).
[10] H. Christenson, Phys. Rev. Lett. **74**, 4675 (1995).
[11] H. Fretwell, J. Duffy, M. Alam, and R. Evans, J. Radioanal. Nucl. Chem **210**, 575 (1996).
[12] M. Glicksman, A. Lupulescu, and M. Koss, in *Free Boundary Problems* (Springer, 2006), pp. 219–230.
[13] S. T. Moerz, K. Knorr, and P. Huber, Physical Review B **85**, 075403 (2012).
[14] P. Lazar and H. Riegler, Phys. Rev. Lett. **95**, 136103 (2005).
[15] H. Kusumaatmaja, R. Lipowsky, C. Jin, R. C. Mutihac, and H. Riegler, Phys. Rev. Lett. **108**, 126102 (2012).
[16] C. Jin and H. Riegler, J. Phys. Chem. (2016), accepted.
[17] Note2, b. Henrich et al. showed that continuum models are adequate for $\geq$ 2 adjacent fluid mono-layers using computer simulation[34].
[18] R. C. Tolman, J. Chem. Phys. **17**, 333 (1949).
[19] J. K. Berg, C. M. Weber, and H. Riegler, Phys. Rev. Lett. **105**, 076103 (2010).
[20] B. Derjaguin and N. Churaev, J. Colloid Interface Sci. **66**, 389 (1978).
[21] W. F. Seyer, R. F. Patterson, and J. L. Keays, J. Am. Chem. Soc. **66**, 179 (1944).
[22] C. J. Adkins, *Equilibrium Thermodynamics* (Cambridge University Press, 1983).
[23] J. G. Dash, A. W. Rempel, and J. S. Wettlaufer, Rev. Mod. Phys. **78**, 695 (2006).

[24]Note3, please note that in our case, $dG_{\mathrm{I}}/dV_{\mathrm{I}}$ is not simply equal to the Laplace pressure, as in other systems[12,35].
[25]Note4, sometimes called the "true" or the "critical" melting temperature.
[26]K. A. Brakke, Exp. Math. **1**, 141 (1992).
[27]M. Dirand, M. Bouroukba, A.-J. Briard, V. Chevallier, D. Petitjean, and J.-P. Corriou, J. Chem. Thermodyn. **34**, 1255 (2002), ISSN 0021-9614.
[28]P. Yi and G. C. Rutledge, J. Chem. Phys. **135**, 024903 (2011).
[29]H. Riegler and R. Köhler, Nat. Phys. **3**, 890 (2007).
[30]C. Delaunay, J. Math. Pures Appl. pp. 309–314 (1841).
[31]J. Eells, Math. Intell. **9**, 53 (1987).
[32]R. Köhler, P. Lazar, and H. Riegler, Appl. Phys. Lett. **89**, 241906 (2006).
[33]C. Merkl, T. Pfohl, and H. Riegler, Phys. Rev. Lett. **79**, 4625 (1997).
[34]B. Henrich, C. Cupelli, M. Santer, and M. Moseler, New J. Phys. **10**, 113022 (2008).
[35]M. E. Glicksman, *Crystal-Melt Interfaces* (Springer New York, New York, NY, 2011), pp. 181–212, ISBN 978-1-4419-7344-3, URL `https://doi.org/10.1007/978-1-4419-7344-3_8`.